# Relative influence of soot oxidation kinetics and subfilter soot-turbulence interactions on soot evolution in turbulent nonpremixed flames

Pavan Prakash Duvvuri<sup>a,\*</sup>, Hernando Maldonado Colmán<sup>a</sup>, Michael E. Mueller<sup>a</sup>

<sup>a</sup>Department of Mechanical and Aerospace Engineering, Princeton University, Princeton, NJ 08544, USA

## Abstract

Oxidation of soot is a critical process in determining the evolution of soot in turbulent reacting flows. On the one hand, the kinetic rates of soot oxidation remain one of the most significant uncertainties in soot models. On the other hand, turbulent transport plays a significant role in the distribution of soot with respect to the flame structure so the location of soot in regions where oxidation can actually occur. The objective of this work is to assess the relative importance of small-scale turbulent transport and oxidation kinetics on the prediction of soot evolution in turbulent nonpremixed flames. A series of Large Eddy Simulations has been performed in a turbulent nonpremixed piloted jet flame of ethylene and air using a series of soot subfilter PDF models (with different assumptions regarding the small-scale turbulent transport of soot) and a series of kinetic rates for soot oxidation (with differences in kinetic rates for both OH and O2 oxidation). Similar to previous work, the results show that accounting for the disappearance of soot in lean mixtures due to soot oxidation is extremely important to avoid excessive "spurious oxidation" of soot otherwise artificially present in lean mixtures. In addition, the sensitivity to soot oxidation kinetics is found to be significantly less important than this effect. However, once this effect is taken into account in the soot subfilter PDF, the sensitivity to soot oxidation kinetics becomes rather significant compared to further refinements to the soot subfilter PDF models. More specifically, the assumption in the soot subfilter PDF models whether soot oxidation is infinitely fast or finite rate compared to small-scale turbulent transport is a less significant model sensitivity compared to the sensitivity to the kinetic rates of soot oxidation. Furthermore, oxidation by OH and O2 are revealed to play fundamentally different roles in soot evolution.

Keywords: Soot oxidation; Soot subfilter PDF; Soot-turbulence-chemistry interactions; Large Eddy Simulation

Current affiliation of corresponding author: Indian Institute of Technology Bombay

<sup>\*</sup>docmech8@gmail.com

### 1. Introduction

Soot formation, growth, and oxidation in turbulent combustion involve complex chemical kinetics in both the gas-phase and the particle-phase as well as complex, nonlinear interactions with turbulent flow. As a result, modeling soot evolution in turbulent combustion requires a deep understanding of these phenomena and physics-based models capable of capturing these effects. Numerous modeling efforts have been undertaken by the soot modeling community to understand the statistical representation of soot, the soot physiochemical processes (including inception, growth, and oxidation), the kinetics of these processes, and the transport of soot at different scales. This study focuses on the small-scale interactions of turbulent transport of soot with soot oxidation kinetics and their relative sensitivities in soot predictions in turbulent reacting flows.

The oxidation of soot predominantly happens through surface reactions with hydroxyl radicals OH and molecular oxygen  $O_2$ . The oxidation by OH is generally modeled using a simple collision efficiency, first proposed by Neoh et al. [1], and the oxidation by O<sub>2</sub> is generally modeled using some activation barrier without [2] or with [3] a further dependence on the surface reactivity of soot particles. The specific form of the kinetic rates and and their values have been subjected to considerable variation throughout the literature [4-6] and remain one of the most significant uncertainties in soot models. Guo et al. [6] recently proposed a set of optimized rates for both OH and O<sub>2</sub> oxidation by fitting rates to twelve experimental datasets. Compared to state-of-the-art oxidation models, these optimized rates suggested a decrease in the collision efficiency for OH oxidation and an optimized activation barrier for O2 oxidation. These rates have previously been assessed in a turbulent nonpremixed piloted jet flame of natural gas and air by Schiener and Lindstedt [7] and shown to be a secondary concern within a RANS-based modeling framework using an acetylene-based soot inception model. However, in this work, the optimized rates proposed by Guo et al. [6] have been revisited in the context of Large Eddy Simulation (LES) and a more detailed PAH-based soot inception model.

Direct Numerical Simulations (DNS) of turbulent nonpremixed sooting flames [8–10] have suggested that soot has an intermittent nature due to turbulence. In LES, this unresolved intermittency has been modeled using a presumed subfilter Probability Density Function (PDF) model for soot that divides the subfilter soot structure into a non-sooting mode and a sooting mode [11]. At the same time, soot also has a strong dependence on the mixture fraction Z and its dissipation rate  $\chi$ . DNS [8–10] and experiments [12] have both shown that soot is generally confined to richer values of mixture fraction. This confinement is due to soot inception and PAH-based growth at very rich mixture fractions, acetylene-based surface growth at moderately rich mixture fractions, and ox-

idation at leaner mixture fractions. The time scales of inception and growth are typically very long, but the time scales of oxidation can be quite fast. As a result, the soot formed in rich mixtures is transported towards leaner mixtures where it is rapidly oxidized. Based on these observations, Yang et al. [13] introduced a dependence on mixture fraction in the sooting mode of the soot subfilter PDF by assuming that soot exists only in regions of the flame where growth is faster than oxidation; functionally, the sooting mode is only activated beyond a cut-off value of mixture fraction at which the oxidation and growth rates are equal. Berger et al. [14] extended this model to account for a more complex structure in the sooting mode but retained the same dependence on mixture fraction. However, since the soot subfilter PDF model of Yang et al. [13] assumes soot does not exist in regions where oxidation is faster than growth, the model implicitly assumes that oxidation kinetics are infinitely fast compared to turbulent transport. This assumption would not be justified in cases where oxidation kinetics and mixing happen at similar characteristic timescales such as in smoking flames. Therefore, Maldonado Colmán et al. [15] proposed an improved subfilter model for finite-rate oxidation where the sharp cut-off value of the mixture fraction is replaced with a gradual transition in mixture fraction, the width of which is based upon the relative rates of oxidation and transport, thereby allowing for leakage of soot into the lean part of the flame. The modeling efforts by Yang et al. [13] and Maldonado Colmán et al. [15] have previously shown that accounting for the dependence of the sooting mode on mixture fraction is exceptionally important. The original marginal soot subfilter PDF without accounting for the dependence on mixture fraction can underpredict soot by at least an order of magnitude due to "spurious oxidation" of soot at lean mixture fractions.

Two distinct model components therefore substantially impact the predicted oxidation rate of soot in turbulent flames: the soot subfilter PDF and the kinetic rates of soot oxidation. The objective of this work is to understand the relative importance of these two effects and answer a relatively simple question: 'How significant are the uncertainties in the oxidation kinetic rates compared to the variation due to the soot subfilter PDF models?' To address this issue, LES have been performed for a turbulent nonpremixed piloted jet flame using two sets of oxidation kinetic rates and three soot subfilter PDF models. In the next Section, the modeling framework, including the soot subfilter PDF models and the oxidation kinetic rates, are detailed. Then, the test configuration, a well studied turbulent nonpremixed piloted jet flame of ethylene and air, is described along with the computational infrastructure. Finally, the results of the sensitivity study are presented before drawing conclusions.

# 2. Modeling framework

### 2.1. Combustion and soot models

The Radiation Flamelet/Progress Variable (RFPV) approach of Mueller and Pitsch [16] has been used to model combustion. In this model, the detailed flame structure is decoupled from the turbulent flow field and is calculated a priori and stored in a database which is accessed during LES. The reliance of the combustion modeling framework on a flamelet model for nonpremixed combustion is an approximation but sufficiently accurate for laboratory-scale turbulent nonpremixed flames as considerd in this work, as has been shown by Han et al. [17] compared with a Transported PDF model. The RFPV database consists of solutions to the steady nonpremixed flamelet equations with radiative heat losses [13]. The effective Lewis numbers for each species are modeled with the Strain Sensitive Transport Approach (SSTA), in which the species (PAH) with slow chemistry and confined to small length scales retain their molecular Lewis numbers [18]. Each flamelet solution in the database is convoluted with a beta distribution for the subfilter PDF of the mixture fraction, and the final database is tabulated as a function of the filtered mixture fraction  $\widetilde{Z}$ , subfilter mixture fraction variance  $Z_v$ , filtered progress variable  $\widetilde{C}$ , and filtered heat loss parameter  $\widetilde{H}$ .

Soot has been modeled using the bivariate (VS:Volume-Surface Area) Hybrid Method of Moments (HMOM) [19-21] using the first-order moments and the number density of incipient soot particles. The gas-phase contributions to the soot source terms are tabulated in the RFPV database, and the soot source terms are computed during the LES as part of the solution of the filtered moment transport equations, which are explicitly solved in LES. To account for the slow chemistry of PAH, a transport equation is also solved for a representative lumped PAH to obtain the PAH mass fraction. While the current soot model does take into account the fractal morphology of soot aggregates, there are of course other phenomena in more complex soot models (e.g., detailed soot particle reactivity) that are not considered. These soot models are more expensive, and their application to and assessment in turbulent flames is left as an area for future work.

More details about the combustion and soot models can be found in previous works [11, 13, 15, 16, 18–20].

# 2.2. Soot subfilter PDF models

Small-scale interactions between soot, turbulence, and chemistry have been modeled using a presumed PDF approach. A density-weighted filtered quantity  $\tilde{Q}$  (for example, a source term) is closed through convolution against a density-weighted joint subfilter PDF  $\tilde{P}$  of the thermochemical variables  $\xi_k$  (that is,

the mixture fraction Z, progress variable C, and heat loss parameter H) and the soot scalars  $M_j$  (that is, the moments and the number density of incipient soot particles):

$$\widetilde{Q}(\widetilde{\xi}_k, \overline{M}_j) = \iint Q(\xi_k, M_j) \widetilde{P}(\xi_k, M_j) d\xi_k dM_j .$$
(1

This joint subfilter PDF can be represented by the product of a thermochemical PDF and a conditional soot PDF. To represent the intermittent nature of soot, the conditional soot PDF is divided into a sooting mode  $\widetilde{P}_{\rm NS}$ , and a non-sooting mode  $\widetilde{P}_{\rm NS}$ , with the weight of the non-sooting mode given by the subfilter intermittency  $\omega$  [11]:

$$\widetilde{P}(M_i|\xi_k) = \omega \widetilde{P}_{NS} + (1 - \omega) \widetilde{P}_S.$$
 (2)

The non-sooting and sooting modes are represented by delta functions:

$$\widetilde{P}_{\mathrm{NS}} = \delta\left(M_{j}\right) \,, \tag{3}$$

and

$$\widetilde{P}_{S} = \delta \left( M_{j} - M_{j}^{*} \right) , \qquad (4)$$

respectively, where  $M_j^*$  is such that  $\overline{M}_j$  is obtained upon convolution against the joint subfilter PDF. The specific form of  $M_j^*$  depends on the particular form of the subfilter PDF, and the following three subfilter PDF models have been considered in this work.

*Marginal*: Proposed by Mueller and Pitsch [11], the marginal model simplifies the subfilter PDF by assuming that the timescales required for soot are slow compared to the thermochemical quantities. The marginal model assumes no dependence of the sooting mode on the thermochemical quantities, and the conditional PDF is simply the marginal PDF:

$$\widetilde{P}\left(M_{i}|\xi_{k}\right) = \widetilde{P}\left(M_{i}\right). \tag{5}$$

Infinitely Fast Oxidation (IFO): In a later work, Yang et al. [13] argued that, although the timescales required for soot inception and growth are indeed slow, the timescales of soot oxidation are not and instead comparable to that of the gas-phase chemistry. Furthermore, the oxidation rate coefficients are very large for lean mixture fractions. As a result, the marginal subfilter PDF model results in "spurious oxidation" of soot at very lean mixtures due to an absence of mixture fraction dependency of the subfilter model. To account for this, Yang et al. [13] proposed activating the sooting mode only beyond a cut-off value of the mixture fraction  $Z_{\mathrm{soot}}$ . This cut-off mixture fraction is selected to be the mixture fraction at which the acetylene-based surface growth rate coefficient  $k_{\rm sg}$  is as fast as the soot oxidation rate coefficient  $k_{ox}$ . This cut-off mixture fraction varies with the mixture fraction dissipation rate (as well as heat losses), that is,

$$Z_{\text{soot}}(\chi_{\text{st}}) = Z(\chi_{\text{st}} | k_{\text{ox}} = k_{\text{sg}})$$
 (6)

and is implemented using a Heaviside function for the sooting mode in the soot subfilter PDF as

$$M_j^*(Z, \chi_{\rm st}) = M_j^{**} H(Z - Z_{\rm soot})$$
 (7)

As detailed by Yang et al. [13],  $M_j^{**}$  is selected such that  $M_j^*$  recovers  $\overline{M}_j$  upon convolution with the joint subfilter PDF.

Finite-Rate Oxidation (FRO): The IFO model accounts for the absence of soot at leaner mixture fractions, but this inherently assumes that oxidation kinetics are infinitely fast compared to turbulent mixing since the cut-off in mixture fraction is sharp. Maldonado Colmán et al. [15] relaxed this assumption, replacing the sharp cut-off in mixture fraction with a gradual transition with a shape q given by

$$g\left(Z, \chi_{\rm st}\right) = \frac{1}{2} + \frac{1}{2} \tanh\left(\frac{Z - Z_{\rm soot} + \Delta Z/2}{\Delta Z/2}\right), \tag{8}$$

where  $\Delta Z$  represents the width of the gradual transition in mixture fraction space. This width is determined by comparing the local relative motion of diffusionless soot particles with respect to the flame (using mixture fraction iso-surface displacement speed  $V_Z$  [22]) with the local oxidation rate coefficient:

$$\Delta Z = V_Z \left| \nabla Z \right| / k_{\text{ox}} \,. \tag{9}$$

Figure 1 shows the sooting mode  $(\tilde{P}_S)$  for the three subfilter models, along with the rate coefficients of oxidation and growth for an ethylene/air nonpremixed flame at  $\chi_{\rm st} = 10 \, {\rm s}^{-1}$  (steady nonpremixed flamelet equations). Oxidation  $(k_{ox})$  is dominant at leaner mixture fraction values, and the cut-off mixture fraction  $Z_{\rm soot}$  is defined where  $k_{\rm ox}=k_{\rm sg}$ . The marginal model does not depend on mixture fraction so has a significant contribution where the oxidation rate coefficient is very large, leading to "spurious oxidation." Both the IFO and FRO models disappear where oxidation is very fast, with IFO having a sudden change at  $Z_{\text{soot}}$  and FRO having a gradual change near  $Z_{\text{soot}}$ . For these models, this "spurious oxidation" is absent, and, further, FRO allows for leakage of soot into leaner mixtures if the local transport rate is fast enough. As would be expected, the value of  $Z_{\rm soot}$ increases with an increase in  $\chi_{\rm st}$ .

As a final note on the soot subfilter PDF models, where soot is present, there is no explicit presumption of any correlation between soot and mixture fraction. The soot subfilter PDF models only seek to determine where soot is absent (oxidized) in mixture fraction space.

# 2.3. Soot oxidation kinetics

In the soot model, oxidation occurs via OH and  $O_2$ . The default oxidation rate coefficients in the HMOM soot model  $(k_{ox,1})$  are those from Blanquart and Pitsch [5] in which the oxidation rate for OH  $(k_{OH,1})$  is taken from Neoh et al. [1] and the oxidation rate for  $O_2$   $(k_{O_2,1})$  is taken from Kazakov et

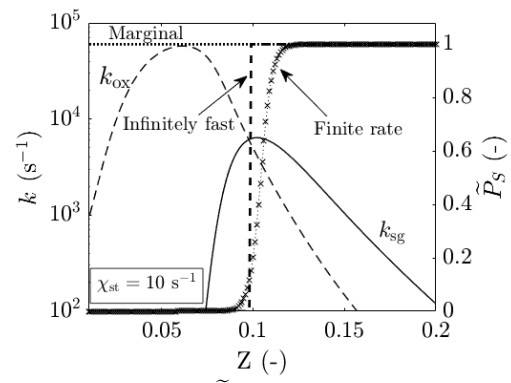


Fig. 1: Sooting mode  $\widetilde{P}_{\rm S}$  of the three soot subfilter PDF models along with the rate coefficients of oxidation  $k_{\rm ox}$  and surface growth  $k_{\rm sg}$ . The conditions correspond to an ethylene/air flame at standard conditions with  $\chi_{\rm st}=10~{\rm s}^{-1}$ .

al. [23]; for the latter rate, the oxidation rate is proportional to the number of radical sites on the soot surface. The number of radical sites is calculated using a steady-state assumption for the radical sites assuming an active site density of  $1.7 \times 10^{19} \, \mathrm{m}^{-2}$ . These default rates will be compared with the optimized oxidation rates  $(k_{\mathrm{ox},2})$  from Guo et al. [6] based on twelve experimental datasets. Table 1 summarizes the key attributes and constants for the two sets of oxidation rates rates considered. To summarize the key differences, the rates of Guo et al. [6] have a lower collision efficiency  $(\eta_{\mathrm{OH}})$  for the oxidation rate for OH  $(k_{\mathrm{OH},2})$  and have an oxidation rate for  $O_2$   $(k_{\mathrm{O2},2})$  that is independent of radical site density and has a higher activation energy.

These two set of oxidation rates  $(k_{\rm ox,1} \text{ and } k_{\rm ox,2})$  have been implemented in flamelet calculations and have been tabulated in the thermochemical database. Figure 2 (top) shows the total oxidation rate coefficients  $(k_{\rm ox} = k_{\rm OH} + k_{\rm O_2})$  along with the constituent rate coefficients of  $O_2$   $(k_{\rm O_2})$  and OH  $(k_{\rm OH})$  in mixture fraction space at a representative dissipation rate. Figure 2 (bottom) further shows the peak values of the oxidation rate coefficients in mixture fraction space at different dissipation rates.

Comparing the two sets of rates, due to a decreased collision efficiency  $(\eta_{\rm OH})$ ,  $k_{\rm OH,2}$  is slower than  $k_{OH,1}$ , and, except for very lean mixtures,  $k_{\rm O2,2}$  is faster than  $k_{\rm O2,1}$  and, due to a larger activation energy, peaks closer to stoichiometric mixture fraction. The differences between the two rates for oxidation by  $O_2$  are most pronounced at rich mixtures (Z>0.15), where  $k_{\rm O2,2}$  is nearly as fast as oxidation by OH while  $k_{\rm O2,1}$  is negligibly small. Additionally, the peak oxidation rates have a very different response to the scalar dissipation rate. For large scalar dissipation rates, oxidation by OH dominates for both sets of rates. However, for small scalar dissipation rates, oxidation by  $k_{\rm O2,2}$  is actually faster than  $k_{\rm OH,2}$ , while the trend is reversed for the other set of rates with

Table 1: Oxidation rate parameters for OH and $O_2$ oxidation in terms of collision efficiency $(\eta)$ and modified Arrhenius form
$(A, n, E)$ , respectively, with units in K, kmol, $m^3$ , and s.

$k_{j}$	$\eta_j$	$A_{j}$	$n_{j}$	$E_{j}$	Radical Site Dependence	Reference
$k_{\mathrm{OH,1}}$	0.13	_	_	_	×	[1]
$k_{\mathrm{OH,2}}$	0.10	_	_	_	×	[6]
$k_{O_2,1}$	_	$2.2 \times 10^{6}$	0.0	31.38	✓	[23]
$k_{\mathrm{O}_2,2}$	_	$1.1 \times 10^{4}$	0.5	195.0	×	[6]

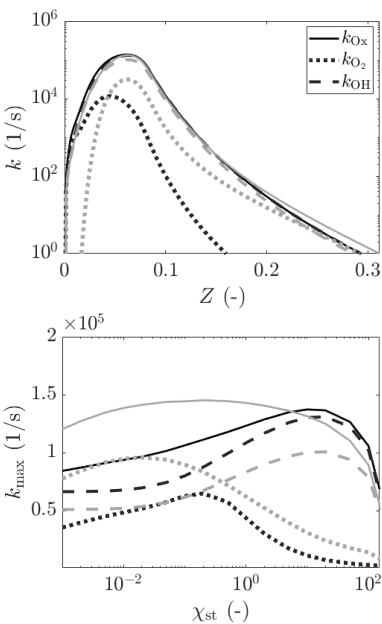


Fig. 2: Top: Oxidation rate coefficients  $(k_{\rm ox}, k_{\rm O_2}, k_{\rm OH})$  at  $\chi_{\rm st}=10~{\rm s^{-1}}$ . Bottom: Peak values of oxidation rate coefficients at different dissipation rates  $(\chi_{\rm st})$ . Black lines are rate coefficients from Blanquart and Pitsch [5], and grey lines are rate coefficients from Guo et al. [6]. The conditions correspond to ethylene/air flames.

 $k_{\mathrm{OH},1}$  faster for all dissipation rates. The behavior of  $k_{\mathrm{O2},2}$  in particular, makes its effect on soot evolution in turbulent nonpremixed flames both more significant and more nuanced than its  $k_{\mathrm{O2},1}$  counterpart, which is more or less always negligible. These differences will be discussed later in the manuscript.

# 3. Configuration and computational details

The Sandia sooting flame [24] is a turbulent non-premixed piloted jet flame operating at atmospheric pressure. The pure ethylene central fuel jet has a jet Reynolds number  ${\rm Re}=20,000,$  with a bulk velocity of  $54.7~{\rm m/s}$  and a diameter  $D=3.2~{\rm mm}.$  The pilot flame is obtained from an ethylene-air premixture at  $\phi=0.9,$  with a thermal power equivalent to 2% of the main jet, and the pilot diameter is  $19.1~{\rm mm}.$  The surrounding air co-flow has a bulk velocity of  $0.6~{\rm m/s}$  to isolate the flame from external perturbations.

LES have been performed using NGA [25, 26], a finite difference solver for low Mach number turbulent reacting flows. The computational domain is the same as previous work [13, 15, 18] and consists of a structured cylindrical grid of  $192 \times 96 \times 32$  points in the streamwise, radial, and circumferential directions, respectively. The dimensions of the domain are  $300D \times 70D$  in the streamwise and radial directions, respectively. The velocity profile for the fuel jet inlet has been obtained from a separate non-reacting periodic pipe flow simulation, and uniform velocities are specified for the pilot and coflow. Turbulent transport has been modeled using Lagrangian dynamic Smagorinsky(-like) models [27, 28].

The RFPV database that is accessed during LES is generated using FlameMaster [29]. The flamelet computations utilize a detailed chemical mechanism [30, 31] with PAH chemistry up to four aromatic rings.

# 4. Results

The modeling framework mentioned in Section 2 and Section 3 has been applied to the Sandia sooting flame for three soot subfilter PDF models (Marginal, IFO, and FRO) and two sets of oxidation rates ( $k_{ox,1}$ from Blanquart and Pitsch [5] and  $k_{ox,2}$  from Guo et al. [6]). The set of oxidation rates  $k_{ox,2}$  have been implemented only with the FRO soot subfilter model due to its superior representation of the small-scale interactions between soot, turbulence, and chemistry and is referred to as FRO-Ox in the figures, but the influence of the oxidation kinetics is not expected to differ significantly with soot subfilter PDF model. The results shown have been averaged over 200 ms. Figure 3 shows the mean temperature along the centerline (left) and for radial profiles at two axial locations with comparison to experimental measurements (center and right). Compared to the other models, the marginal soot subfilter PDF model tends to overpredict the temperature, while the other soot subfilter PDF models are generally in very good agreement with one another and with the experimental measurements. The only influence on the temperature is through the prediction of the soot volume fraction and associated soot radiation, and, as shown subsequently, the marginal model significantly underpredicts the soot volume fraction (consistent with prior work [13, 15]), and reduced soot results in reduced heat losses and an overpredicted temperature.

The mean and RMS soot volume fraction along the

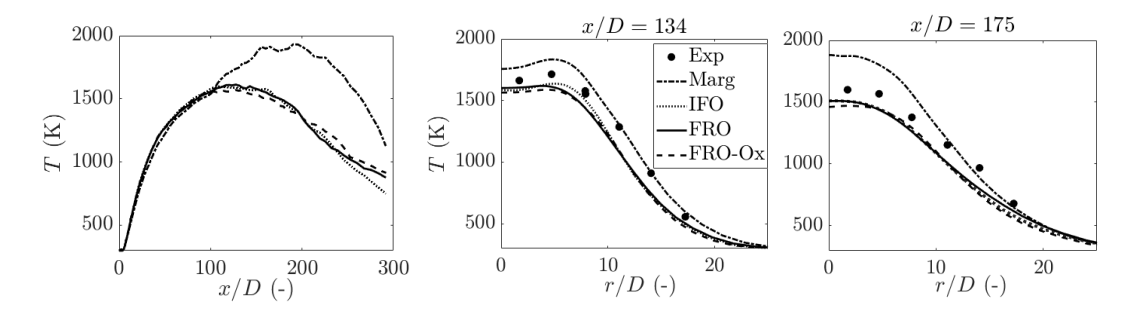


Fig. 3: Mean temperature profile along the centerline (left) and radial profiles at two axial locations (center and right). The experimental data (symbols) is from Kearney et al. [32]. The default oxidation rates are  $k_{\text{OX},1}$ , and the '-Ox' indicates the use of the  $k_{\text{OX},2}$  rates.

centerline are shown in Fig. 4. Figure 5 shows qualitative results of the mean soot volume fraction fields using the four models. Mean mixture fraction isolines are also plotted, where the stoichiometric isoline corresponds to  $Z=Z_{\rm st}=0.0635$ . The results shown for the soot volume fraction are Reynolds averaged, Reynolds filtered quantities since the soot volume fraction is already density-weighted. From Fig. 4, it can be seen that the mixture fraction dependent subfilter models result in a similar order of magnitude of soot compared to the experimental measurements in terms of the maximum (an overprediction of a factor of a few), while as indicated previously, the marginal model severely underpredicts the mean and RMS soot volume fraction (an underprediction by more than one order of magnitude). This underprediction is due to excessive "spurious oxidation" in the marginal soot subfilter PDF as discussed in detail by Yang et al. [13].

From Fig. 5, it can be observed that the FRO model allows for a very slightly wider sooting region compared to the IFO model. Along the centerline (Fig. 4), the most significant difference between the FRO and IFO models for the mean volume fraction is in the soot inception region (40 < x/D < 90), where the mean mixture fraction is relatively close to the cutoff mixture fraction; in this region, the model predictions are slightly influenced by the effect of the gradual transition in the FRO model on the surface growth rate, which is more significant at large mixture fraction dissipation rates. See Maldonado Colmán et al. [15] for further discussion as well as a priori analysis of DNS data that demonstrates the correctness of this effect. Downstream, where the mean mixture fraction is leaner than the cut-off mixture fraction, both models give more or less identical results.

The influence of the soot oxidation kinetics are at the same time very obvious and very subtle. The most obvious effect of the the rates of Guo et al. [6] is the increased maximum mean centerline volume fraction (the increased soot volume fraction in the region 100 < x/D < 200) compared to the rates of Blanquart

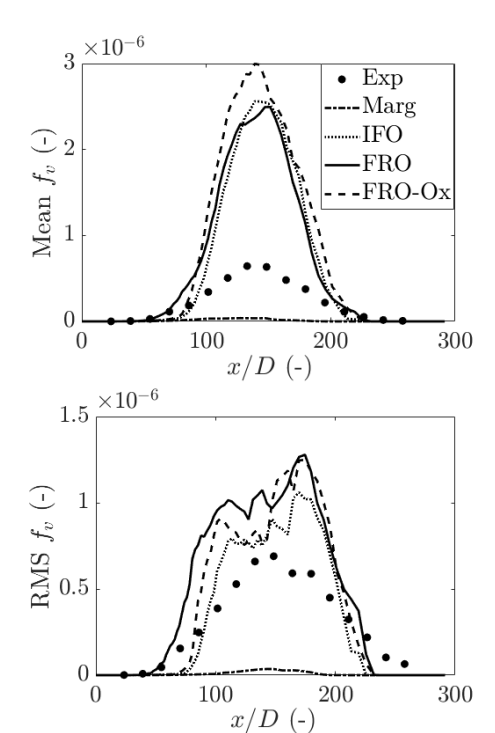


Fig. 4: Mean (Top) and RMS (bottom) soot volume fraction  $(f_v)$  profiles along the centerline. Experimental data is from Zhang et al. [24]. See Fig. 3 for further commentary on legend

and Pitsch [5]. The peak is largely determined by the balance between inception/growth and oxidation, and, at this location where the mean mixture fraction is relatively lean (Fig. 6) and with a relatively large dissipation rate, oxidation by OH dominates with both sets of rates. Since the OH oxidation rate is slower with the rates of Guo et al. [6], the resulting peak mean centerline soot volume fraction is larger. The reduced oxidation rate with the rates of Guo et al. [6] is clearly evident in Fig. 7 (middle) where the radial profile of

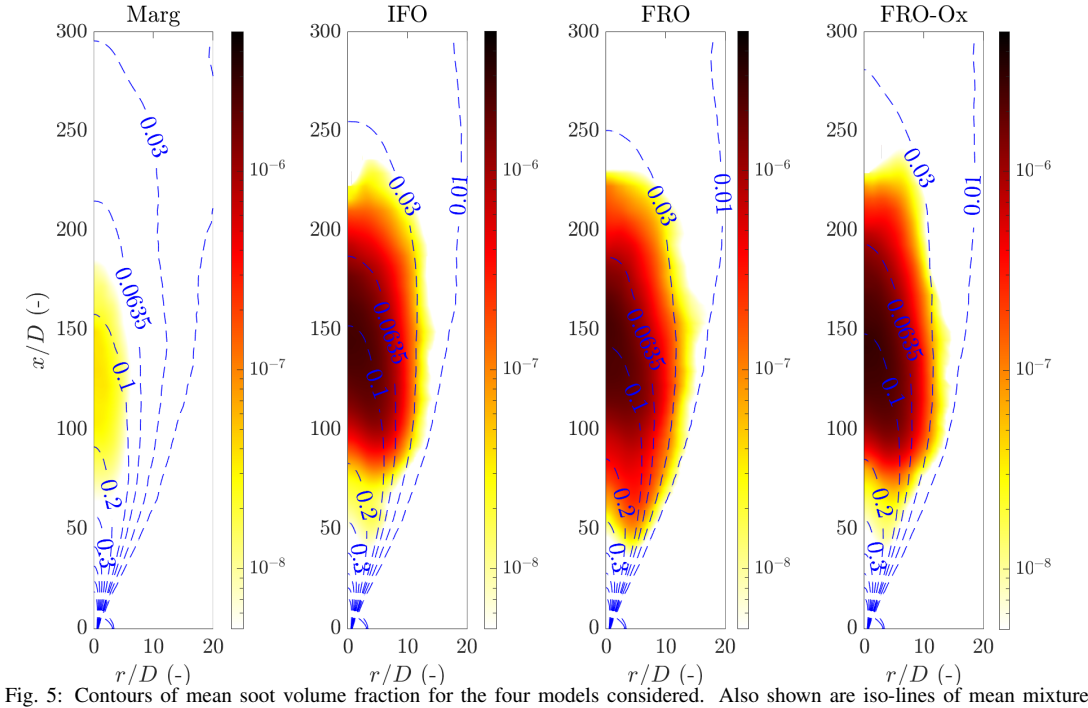


Fig. 5: Contours of mean soot volume fraction for the four models considered. Also shown are iso-lines of mean mixture fraction, and stoichiometric mixture fraction corresponding to the value 0.0635.

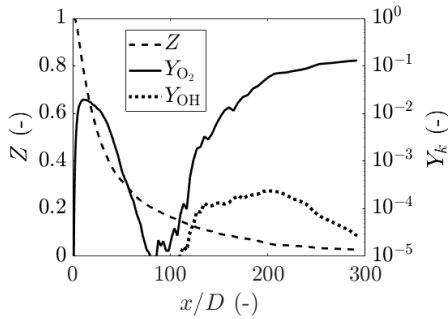


Fig. 6: Mean mixture fraction, oxygen mass fraction, and hydroxyl mass fraction along the centerline for the FRO-Ox case.

the normalized oxidation rate is shown.

There are two additional subtle effects of the rates of Guo et al. [6] compared to the rates of Blanquart and Pitsch [5]. First, as shown in Fig. 4 and Fig. 5, with the rates of Guo et al. [6], the soot volume fraction is lower in the inception region of the flame. In this region, as shown in Fig. 7 (left), inception is actually offset by a faster oxidation rate. In this region, the mean mixture fraction is very rich  $\tilde{Z}>0.2$ , and, according to Fig. 2 (top), oxidation by  $O_2$  becomes competitive with oxidation by OH at these very rich mixture fractions, and its substantially increased rate acts to reduce the soot volume fraction. Second, as shown in Fig. 4, with the rates of Guo et al. [6], the

soot volume fraction is also lower in the far downstream region of the flame  $(x/D{>}200)$ . In this region, the dissipation rate is quite low, and, as shown in Fig. 2 (bottom), oxidation by  $O_2$  becomes dominant at such conditions with the rates of Guo et al. [6] and its faster rate compared to those of Blanquart and Pitsch [5] increases the oxidation rate, as shown in Fig. 7 (right), and decreases the mean soot volume fraction.

Based on the results, two clear conclusions can be drawn. First, the influence of the marginal soot subfilter PDF compared to the soot subfilter PDF models that account for the dependence on mixture fraction is the dominant sensitivity, and the influence of the oxidation kinetic rates is substantially smaller than the elimination of the "spurious oxidation" in the marginal soot subfilter PDF model. Second, however, the influence of the soot oxidation kinetics (FRO versus FRO-Ox in the figures) is more significant than the differences between the FRO and IFO models. In other words, the sensitivity of soot volume fraction predictions to the oxidation kinetics is at least as important as the finer details of the mixture fraction dependence in the soot subfilter PDF model. Translating this conclusion to other combustion modeling frameworks, this likely means that any models affecting subfilter turbulent transport of soot (e.g., subfilter mixing models in the Transported PDF approach) are dominant sensitivities in the prediction of soot evolution in turbulent combustion. Additionally, given that key phenomena are unresolved, this conclusion

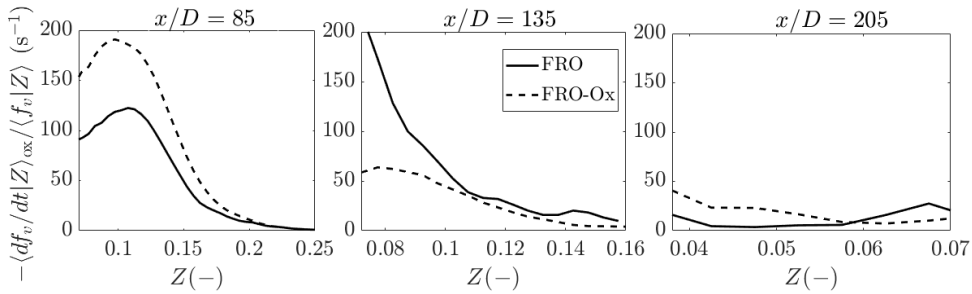


Fig. 7: Normalized conditional mean soot volume fraction source term for oxidation at three different axial locations.

is likely agnostic to LES versus RANS, and the conclusion is also unlikely sensitive to the specific soot modeling framework (e.g., would also apply to a sectional soot model).

# 5. Conclusions

Large Eddy Simulations have been performed for a turbulent nonpremixed piloted jet flame to assess the importance of subfilter soot PDF models and uncertainties in soot oxidation kinetics. Three soot subfilter PDF models were considered, specifically a marginal model (no dependence on mixture fraction), a conditional model that considers the dependence of soot on mixture fraction but makes an implicit assumption that soot oxidation is infinitely fast, and a conditional model that considers the dependence of soot on mixture fraction and can accommodate finite-rate soot oxidation. Two sets of soot oxidation kinetic rates, one baseline set and one with slower oxidation by OH but faster oxidation by O2. The results indicate that the most important sensitivity is the accounting for the dependence of soot on mixture fraction in some form to remove excessive "spurious oxidation" that plagues the marginal soot subfilter PDF model and leads to a severe underprediction of the soot volume fraction. However, the influence of the fine details of the dependence on mixture fraction is relatively less important, and its sensitivity is at most comparable to the sensitivity to the uncertainties in the kinetic rates of soot oxidation. Additionally, the influence of the soot kinetic rates is not as simple as more soot or less soot. The reduced rate of OH oxidation relative to the baseline rates increases the maximum mean soot volume fraction, but the increased rate of O2 oxidation relative to the baseline rates reduces the soot volume fraction in the inception region (rich mixture fractions) and in the far downstream region (low mixture fraction dissipation rates) of the jet flame where O2 oxidation plays an important role with the alternative rates considered.

Improvements in the predictive capability for soot evolution in turbulent reacting flows would therefore benefit from not only improved models for the small-scale interactions between soot, turbulence, and chemistry but also from the reduction in the uncertainties of kinetic rates for oxidation.

# Acknowledgments

The authors gratefully acknowledge funding from ANSYS, Inc. and from the National Science Foundation, Award CBET-2028318. The simulations presented in this article were performed on computational resources supported by the Princeton Institute for Computational Science and Engineering (PISciE) and the Office of Information Technology's High Performance Computing Center and Visualization Laboratory at Princeton University.

# References

- K. G. Neoh, J. B. Howard, A. F. Sarofim, Soot oxidation in flames, in: D. C. Siegla, G. W. Smith (Eds.), Particulate Carbon, 1981, pp. 261–282.
- [2] J. Nagle, R. F. Strikland-Constable, Oxidation of carbon between 1000-2000°C, Proc. Fifth Carbon Conf. (1962) 154–164.
- [3] J. Appel, H. Bockhorn, M. Frenklach, Kinetic modeling of soot formation with detailed chemistry and physics: Laminar premixed flames of C2 hydrocarbons, Combust. Flame 121 (2000) 122–136.
- [4] K. M. Leung, R. P. Lindstedt, W. P. Jones, A simplified reaction mechanism for soot formation in nonpreixed flames, Combust. Flame 87 (1991) 298–305.
- [5] G. Blanquart, H. Pitsch, Analyzing the effects fo temperature on soot formation with a joint Volume-Surface-Hydrogen model, Combust. Flame 156 (2009) 1614–1626.
- [6] H. Guo, P. M. Anderson, P. B. sunderland, Optimized rate expressions for soot oxidation by OH and O2, Fuel 172 (2016) 248–252.
- [7] M. A. Schiener, R. P. Lindstedt, Joint-scalar transported PDF modelling of soot in a turbulent nonpremixed natural gas flame, Combust. Theory Model. 22 (2018) 1134–1175.
- [8] F. Bisetti, G. Blanquart, M. E. Mueller, P. H., On the formation and early evolution of soot in turbulent nonpremixed flames, Combust. Flame 159 (2012) 317– 335
- [9] A. Attili, F. Bisetti, M. E. Mueller, H. Pitsch, Formation, growth, and transport of soot ina threedimensional turbulent non-premixed jet flame, Combust. Flame 161 (2014) 1849–1865.
- [10] A. Attili, F. Bisetti, M. E. Mueller, H. Pitsch, Damk ohler number effects on soot formation and growth in turbulent nonpremixed flames, Combust. Flame 162 (2015) 3437–3445.

- [11] M. E. Mueller, H. Pitsch, Large eddy simulation subfilter modeling of soot-turbulence interactions, Phys. Fluids 23 (2011) 115104.
- [12] O. Park, R. A. Burns, N. T. Clemens, Relationshiop between soot and scalar dissipation rate in the sootinception region of turbulent non-premixed jet flames, Proc. Combust. Inst. 37 (2019) 1057–1064.
- [13] S. Yang, J. K. Lew, M. E. Mueller, Large Eddy Simulation of soot evolution in turbulent reacting flows: Presumed subfilter PDF model for soot-turbulencechemistry interactions, Combust. Flame 209 (2019) 200–213
- [14] L. Berger, A. Wick, A. Attili, M. E. Mueller, H. Pitsch, Modeling subfilter soot-turbulence interactions in Large Eddy Simulation: An a priori study, Proc. Combust. Inst. 38 (2021) 2783–2790.
- [15] H. Maldonado Colmán, A. Attili, M. E. Mueller, Large Eddy Simulation of turbulent nonpremixed sooting flames: Presumed subfilter PDF model for finite rate oxidation, Combust. Flame (2022) Under Review.
- [16] M. E. Mueller, H. Pitsch, LES model for sooting turbulent nonpremixed flames, Combust. Flame 159 (2012) 2166–2180.
- [17] W. Han, V. Raman, M. E. Mueller, Z. Chen, Effects of combustion models on soot formation and evolution in turbulent nonpremixed flames, Proceedings of the Combustion Institute 37 (1) (2019) 985–992. doi:https://doi.org/10.1016/j.proci.2018.06.096.
- [18] S. Yang, J. K. Lew, M. E. Mueller, Large Eddy Simulation of soot evolution in turbulent reacting flows: Strain-Sensitive Transport Approach for Polycyclic Aromatic Hydrocarbons, Combust. Flame 220 (2020) 219–234.
- [19] M. E. Mueller, G. Blanquart, H. Pitsch, Hybrid Method of Moments for modeling soot formation and growth, Combust. Flame 156 (2009) 1143–1155.
- [20] M. E. Mueller, G. Blanquart, H. Pitsch, A joint volume-surface model of soot aggregation with the method of moments, Proc. Combust. Inst. 32 (2009) 785–792.
- [21] M. E. Mueller, G. Blanquart, H. Pitsch, Modeling the oxidation-induced fragmentation of soot aggregates in laminar flames, Proc. Combust. Inst. 33 (2011) 667– 674.
- [22] S. B. Pope, The evolution of surfaces in turbulence, Int. J. Eng. Sci. 26 (1988) 445–469.
- [23] A. Kazakov, M. Frenklach, Dynamic modeling of soot particle coagulation and aggregation: Implementation with the method of moments and application to highpressure laminar premixed flames, Combust. Flame 114 (1998) 484–501.
- [24] J. Zhang, C. R. Shaddix, R. W. Schefer, Design of "model-friendly" turbulent non-premixed jet burners for C2+ hydrocarbon fuels, Rev. Sci. Instum. 82 (2011) 074101.
- [25] O. Desjardins, G. Blanquart, G. Balarac, H. Pitsch, High order conservative finite difference scheme for variable density low Mach number turbulent flows, J. Comput. Phys. 227 (2008) 7125–7159.
- [26] J. F. MacArt, M. E. Mueller, Semi-implicit iterative methods for low Mach number turbulent reacting flows: Operator splitting versus approximate factorization, J. Comput. Phys. 326 (2016) 569–595.
- [27] M. Germano, U. Piomelli, P. Moin, W. H. Cabot, A dynamic subgrid-scale eddy viscosity mode, Phys. Fluids A 3 (1991) 1760–1765.
- [28] C. Meneveau, T. S. Lund, W. H. Cabot, A Lagrangian

- dynamic subgrid-scale model of turbulence, J. Fluid Mech. 319 (1996) 353–385.
- [29] H. Pitsch, FlameMaster, a C++ computer program for 0D combustion and 1D lamianr flame calculations. URL https://www.itv.rwth-aachen.de/ downloads/flamemaster/
- [30] G. Blanquart, H. Pitsch, Chemical mechanism for high temperature combustion of engine relevant fuels with emphasis on soot precursors, Combust. Flame 156 (2009) 588–607.
- [31] K. Narayanaswamy, G. Blanquart, H. Pitsch, A consistent chemical mechanism for oxidation of substituted aromatic species, Combust. Flame 157 (2010) 1879– 1898
- [32] S. P. Kearney, D. R. Guidenbecher, C. Winters, P. A. Farias, T. W. Grasser, J. C. Hewson, Temperature, oxygen, and soot-volume-fraction measurements in a turbulent C2H4-fueled jet flame, Tech. rep., SAND2015-7968 (2015).